

Metamorphic conditions during formation of a metapelitic sillimanite-garnet gneiss from Clemence Massif, Prince Charles Mountains, East Antarctica

A. F. Corvino, S. D. Boger, and C. J. L. Wilson

School of Earth Sciences, The University of Melbourne, Victoria, 3010, Australia

Abstract The pressure (P) and temperature (T) conditions during metamorphism of a metapelitic sillimanite-garnet gneiss from Clemence Massif, Antarctic Prince Charles Mountains, are estimated using mineral abundance information and petrogenetic P - T pseudosections computed in the chemical system $\text{MnO-N}_2\text{O-CaO-K}_2\text{O-FeO-MgO-Al}_2\text{O}_3\text{-SiO}_2\text{-H}_2\text{O-TiO}_2\text{-Fe}_2\text{O}_3$ (MnNCKFMASHTO). Calculated mineral equilibria for the appropriate bulk composition predict that the observed assemblage, of K-feldspar-garnet-quartz-sillimanite-biotite-ilmenite-rutile, stabilised at approximately 8–9 kbar and 760–790°C. Reaction microstructures are rare, but the preservation of relic spinel inclusions in garnet indicates an earlier low- P , high- T component and possible anticlockwise path.

Citation: Corvino A. F., S. D. Boger, and C. J. L. Wilson (2007), Metamorphic conditions during formation of metapelitic sillimanite-garnet gneiss from Clemence Massif, Prince Charles Mountains, East Antarctica, in *Antarctica: A Keystone in a Changing World – Online Proceedings of the 10th ISAES*, edited by A.K. Cooper and C.R. Raymond et al., USGS Open-File Report 2007–1047, Short Research Paper 062, 9 p.; doi:10.3133/of2007-1047.srp062

Introduction

In the central Antarctic Prince Charles Mountains (PCM), between latitudes 72° S and 72°30' S, the Clemence Massif (Fig. 1) forms the largest exposure of a predominantly Late Proterozoic/Early Palaeozoic age crustal belt. This belt also includes Mounts Johns and Izabelle, Shaw Massif, Bosse and Ely Nunataks and Lawrence Hills, that have been previously correlated with Clemence Massif on the basis of compatible ~1000 Ma Rb-Sr whole-rock ages for felsic gneisses, similar structural styles and lack of intrusive mafic dykes (Tingey et al., 1981; Mikhalsky et al., 2001).

Recent U-Pb zircon dating by Corvino et al. (2005) indicates that the Clemence Massif consists of 1060 million year old felsic orthogneiss structurally overlain by, and locally interleaved with, paragneisses of uncertain age all reworked under granulite-facies conditions at ~1000 and/or ~500 million years ago. Importantly, gneisses from this massif preserve evidence for coexistence of both ~1000 Ma and ~500 Ma dates in single zircons, although it is unclear which of these dates accurately reflects the principal metamorphic event. At this point, granulite-facies reworking at Clemence Massif may be related to either of the ~1000 Ma (Grenvillian) or ~500 Ma (Pan-African) tectonic events that are widely recognised in East Antarctica (amongst others Krynauw, 1996 and Yoshida et al., 2003). Furthermore, the possible superimposition of these two events throughout the central region of the PCM is an unresolved matter of concern.

In this paper, we identify the physical conditions of metamorphism for Clemence Massif on the basis of phase relations recorded in a rare metapelitic gneiss, with the aim of further illuminating the relative importance of the ~1000 Ma and ~500 Ma events at this location. Our approach utilises petrogenetic pseudosections, along with a knowledge of mineral abundances and the relevant bulk composition, following closely the method and logic of Stüwe and Powell (1995).

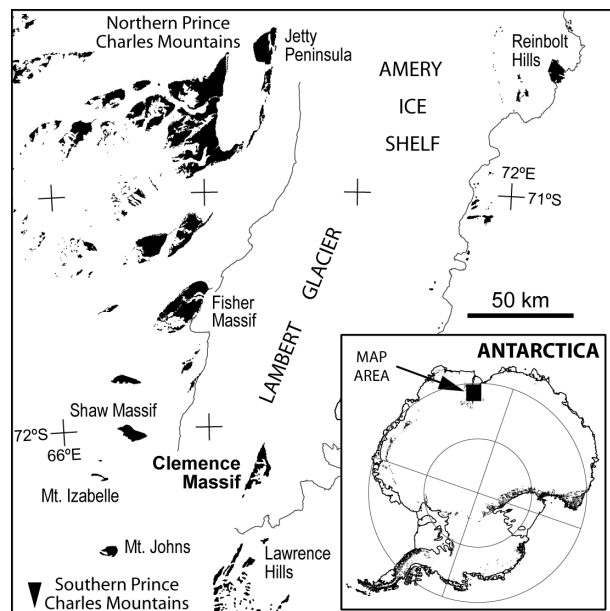


Figure 1. Map showing the location of Clemence Massif in the Prince Charles Mountains, Antarctica.

Petrography and mineral chemistry

The sample in this study (Fig. 2) was collected from a metre-thick layer of metapelitic gneiss located on the east side of Clemence Massif, at latitude 72°11'55" S and longitude 62°49'26" E. It has a fabric formed by layers of preferably oriented sillimanite that anastomose about garnet poikiloblasts and alternate with perthite-rich leucosome domains (~5 mm thick), which are often tapered and discontinuous. The sillimanite is oriented sub-parallel to the principal foliation at Clemence Massif that is typically defined by a gneissose and migmatitic layering with regular dip of ~40° towards the southwest (McLeod, 1959; Tingey et al., 1981; Corvino et al., 2005).

The mineral assemblage consists of perthitic K-feldspar (32 vol.%), garnet (24 vol.%), quartz (20 vol.%), sillimanite (19 vol.%), biotite (3 vol.%) and ilmenite (2 vol.%), along with minor rutile and relic spinel that

together comprise <0.3% of the rock volume (Table 1). Chemical data for the minerals are given in Appendix B (Tables B1 and B2).

K-feldspar has a grain size of 500–1500 μm and is mostly perthite comprising ~82 mol.% orthoclase ($=100\cdot\text{K}/\text{Ca}+\text{Na}+\text{K}$) and ~18 mol.% albite ($=100\cdot\text{Na}/\text{Ca}+\text{Na}+\text{K}$), with <1 mol.% anorthite ($=100\cdot\text{Ca}/\text{Ca}+\text{Na}+\text{K}$). Adjacent grain boundaries are straight, or cusped-and-lobate where they are in contact with quartz which forms irregular shapes and fine bleb-type growths (25–250 μm). Both K-feldspar and quartz may be elongate and host fine sillimanite inclusions where they are associated with sillimanite masses. Incipient subgrains are evident in quartz.

Garnet is an almandine–pyrope (Fe–Mg) solid solution, with 71 mol.% almandine ($=100\cdot\text{Fe}^{\text{T}}/\text{Fe}^{\text{T}}+\text{Mg}+\text{Ca}+\text{Mn}$), and contains <5 mol.% total spessartine ($=100\cdot\text{Mn}/\text{Fe}^{\text{T}}+\text{Mg}+\text{Ca}+\text{Mn}$) and grossular ($=100\cdot\text{Ca}/\text{Fe}^{\text{T}}+\text{Mg}+\text{Ca}+\text{Mn}$). Significant compositional zoning is not evident. Most garnet forms irregular-to-globular, fractured poikiloblasts (2–5 mm diameter) with inclusions of quartz, ilmenite and biotite; the inclusion sizes are <250 μm and more rounded than their counterparts in the adjoining matrix. Inclusion trails are uncommon, but they do occur in a few remarkable garnets as shown in Figure 3a. The trails are oriented obliquely to the external fabric, as defined by sillimanite, and do not continue into it. This suggests that some garnet growth probably preceded development of the sillimanite-defined fabric (cf. Johnson and Vernon, 1995).

Sillimanite may be intergrown with garnet poikiloblast edges, but it mostly anastomoses around these. It occurs as fibrolitic masses and (relatively) large prismatic crystals, with lengths ranging from 50 μm to 3000 μm , and length/width indices of about 10. Several of the largest sillimanite grains are gently kinked and show undulatory extinction. Some are conspicuously misaligned with respect to the main foliation, as shown in Figure 3b, and possibly reflect late growth.

Biotite is a phlogopite–annite solid solution with molar $\text{Mg}/\text{Fe}^{\text{T}}+\text{Mg}$ ratios of 0.52–0.73. Titanium contents range from 0.37 to 0.71 atoms per 22 oxygens, decreasing in accordance with increasing $\text{Mg}/\text{Fe}^{\text{T}}+\text{Mg}$. The majority

of biotite occurs as dispersed laths <1 mm in contact with all matrix phases, or forms irregular late growths between sillimanite crystals and garnet fractures. Some biotite hosts sagenitic rutile as shown in Figure 3c. The rutile forms asterisk-shaped aggregates of acicular inclusions <100 μm in length and intersecting at angles of ~60° analogous to descriptions by Shau et al. (1991). Rutile is also present in the matrix and as inclusions within garnet.

Ilmenite is mostly pure FeTiO_3 with only 0.01 Mn apfu (per 6 O). Like biotite, it appears as rectangular shapes disseminated throughout the matrix or as irregular growths interspersed with sillimanite (Fig. 3b).

Spinel is primarily a hercynite–gahnite–spinel solid solution, with as much as 27 mol.% gahnite ($=100\cdot\text{Zn}/\text{Fe}^{\text{T}}+\text{Mg}+\text{Zn}$). It is absent from the matrix and occurs only within garnet porphyroblasts as relic bleb-shaped inclusions <250 μm (Fig. 3c).

All phases, excluding spinel, are assumed to have crystallised in local equilibrium. Notably absent phases are plagioclase and cordierite.

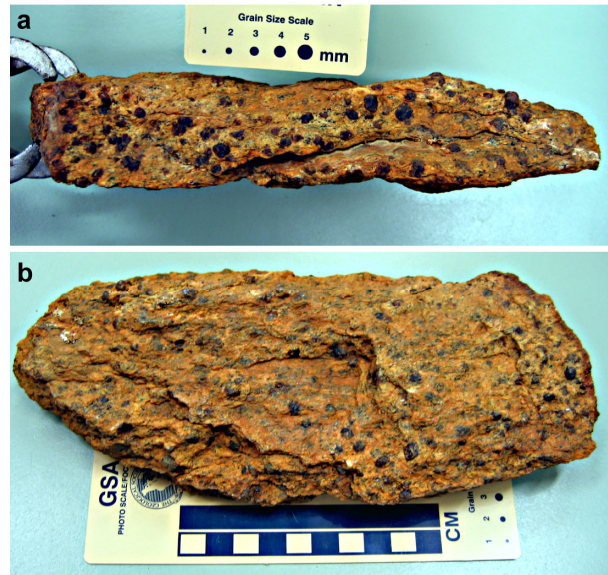


Figure 2. Photographs of the study sample. (a) Sub-parallel, and (b) oblique to the principal foliation. The porphyroblasts are garnet.

Table 1. Petrographic data for the metapelitic gneiss in this study. Point counts were made of two thin-sections (i and ii) using a graduated mechanical stage and sampling interval of 667 μm (Glagolev-Chayes method, see Carver, 1971). Molar abundances of each phase were calculated by dividing vol.% by molar volumes, and multiplying by the number of oxides per mineral formula (using the data given in Appendix A). The values are recalculated to 100%.

| | K-feldspar | quartz | sillimanite | garnet | ilmenite | biotite | rutile | Totals |
|------------------|------------|--------|-------------|--------|----------|---------|--------|--------|
| Point counts i | 439 | 295 | 266 | 195 | 24 | 27 | 4 | 1250 |
| Point counts ii | 372 | 201 | 199 | 409 | 19 | 49 | 1 | 1250 |
| i+ii | 811 | 496 | 465 | 604 | 43 | 76 | 5 | 2500 |
| Vol.% (i+ii) | 32.4 | 19.8 | 18.6 | 24.2 | 1.7 | 3.0 | 0.2 | 100 |
| Mol. abundance % | 26.2 | 19.2 | 16.4 | 32.5 | 2.4 | 3.1 | 0.2 | 100 |
| Wt.% | 27.0 | 16.9 | 19.5 | 30.7 | 2.6 | 2.9 | 0.3 | 100 |

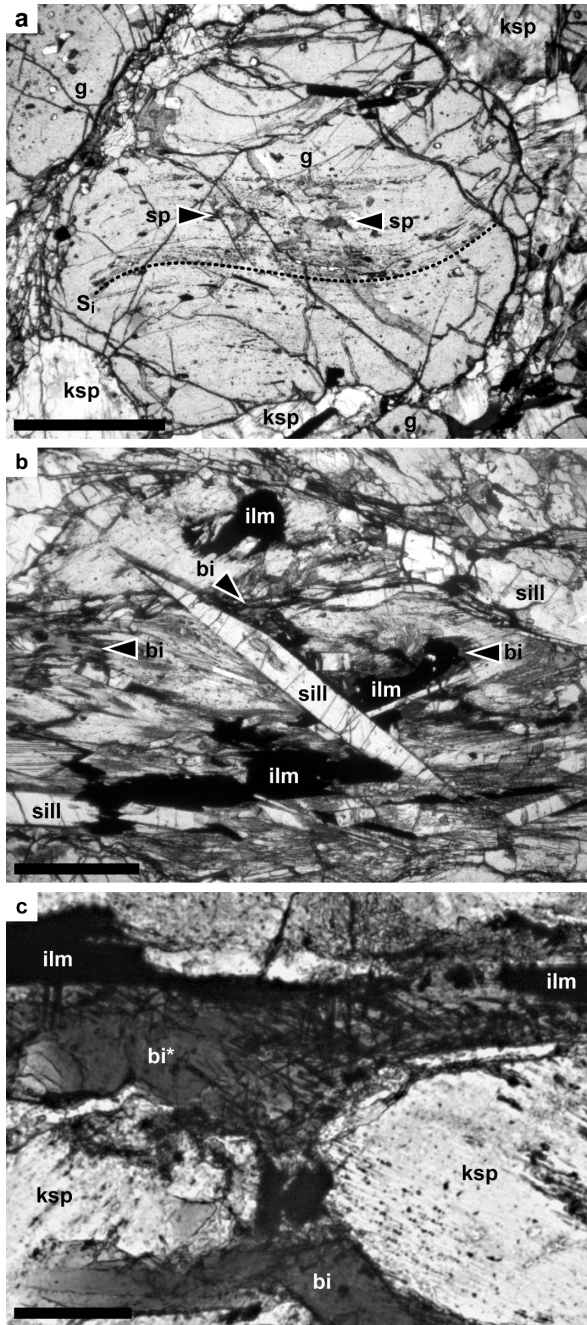


Figure 3. Microphotographs. (a) Garnet poikiloblast with rare inclusion trail (S_i) defined by an opaque phase, probably ilmenite, and sparse hercynite blebs indicated by arrows. Scale bar ~ 2 mm. (b) Aggregates of fibrolitic sillimanite and a few larger sillimanite crystals with lesser ilmenite and biotite. Scale bar ~ 1 mm. (c) Late biotite with sagenitic rutile (bi^*). Scale bar ~ 100 μm .

Bulk chemical composition

A first approximation of the bulk rock composition was made using mineral abundances (Table 1) and chemical data (Tables B1 and B2) following the petrographic method of Friedman (1960). The result is shown in Table 2. Ferric iron contents were considered in

this calculation by assuming Fe^{3+}/Fe^T ratios of 0.08 for biotite (Guidotti and Dyar, 1991), and 0.05 for ilmenite based on example fractions from normal terrestrial rocks (~ 0.10 , Deer et al., 1992) and Fe^{3+} depleted granulites (≤ 0.01 , Cesare et al., 2005). Fe^{3+} in garnet was assumed to be negligible (after Dyar et al., 2002).

An independent chemical analysis was also undertaken using the SPECTRO XLAB2000 X-ray Fluorescence Spectroscopy (XRF) facility at Macquarie University, Australia. Major oxide abundances, obtained for a 50 gram powder aliquot, are given in Table 2. In comparison to the petrographic based calculation, the XRF results show greater Si, K and Na contents, and lesser Al, Fe, Mg and Ti contents, that suggests a slightly higher leucosome:melanosome ratio.

Overall, the metapelitic gneiss has relatively low molar $MgO/(MgO+FeO)$ value of 0.27, which clearly reflects almandine abundance and composition (Table B1), and high Al_2O_3 content (cf. Sheraton, 1980). About half of the total Al_2O_3 (15.10 mol.%) occurs in sillimanite, with the remainder accounted for largely by garnet followed by K-feldspar. K-feldspar is the main source of total K_2O (3.18 mol.%) and Na_2O (0.93 mol.%), and minor CaO (0.41 mol.%) which is also included in garnet. Titania (1.03 mol.%) is partitioned into ilmenite, biotite and rutile. The minor amount of MnO (0.11 mol.%) must occur mainly in garnet and ilmenite based on microprobe analyses (Appendix B).

The estimated amount of Fe_2O_3 is 0.10 mol.%. This value is considered to be realistic because biotite and ilmenite, likely Fe^{3+} bearing phases, constitute only a very small amount of the rock volume ($< 5\%$). Assuming higher Fe^{3+}/Fe^T ratios of say 0.16 for biotite, and 0.10 for ilmenite, in the petrographic calculation increases the total Fe_2O_3 content to only ~ 0.20 mol.%.

Since mostly anhydrous phases are preserved, the H_2O content is undoubtedly low in accord with significant melt loss from the metapelite system (cf. Fyfe, 1973; Powell, 1983). A provisional estimate of 1.98 mol.% was made for H_2O using the wt.% Loss On Ignition (LOI) of volatile species recorded by the XRF analysis.

P-T estimates from petrogenetic pseudosections

Calculations of mineral equilibria were made in the system $MnO-N_2O-CaO-K_2O-FeO-MgO-Al_2O_3-SiO_2-H_2O-TiO_2-Fe_2O_3$ (MnNCKFMASHTO) using the computer software THERMOCALC (Powell and Holland, 1988; Powell et al., 1998; upgrade 3.25) and the internally-consistent thermodynamic dataset of Holland and Powell (1998; update Nov. 2003). Phases considered were biotite, cordierite, garnet, ilmenite, K-feldspar, liquid (silicate melt), muscovite, plagioclase, quartz, rutile, sillimanite and spinel. The activity-composition ($a-x$) relationships used for biotite and ilmenite follow White et al. (2005); garnet, Zeh and Holness (2003); spinel, White et al. (2002); muscovite, Coggon and Holland (2002); K-feldspar, plagioclase and liquid (melt), White et al. (2001), and; cordierite, Maher et al. (1997).

Table 2. Bulk composition data for the metapelitic gneiss from Clemence Massif.

| | SiO ₂ | TiO ₂ | Al ₂ O ₃ | Fe ₂ O ₃ | FeO | MnO | MgO | CaO | Na ₂ O | K ₂ O | P ₂ O ₅ | LOI | Total |
|---------------------------|------------------|------------------|--------------------------------|--------------------------------|--------------|-------------|-------------|-------------|-------------------|------------------|-------------------------------|-------------|---------------|
| Petrographic method* wt.% | 54.80 | 1.65 | 24.25 | 0.26 | 11.66 | - | 2.76 | - | 0.61 | 4.01 | - | - | 100.00 |
| XRF wt.% | 58.67 | 0.81 | 21.59 | 9.97 | - | 0.12 | 1.71 | 0.34 | 1.11 | 4.91 | 0.09 | 0.53 | 99.85 |
| XRF§ wt.% | 58.76 | 0.81 | 21.62 | 0.22 | 9.75 | 0.12 | 1.71 | 0.34 | 1.11 | 4.92 | 0.09 | 0.53 | 100.00 |
| Average wt.% | 56.78 | 1.23 | 22.94 | 0.24 | 10.70 | 0.12 | 2.24 | 0.34 | 0.86 | 4.46 | 0.09 | 0.53 | - |
| Mol.% | 63.40 | 1.03 | 15.09 | 0.10 | 9.99 | 0.11 | 3.72 | 0.41 | 0.93 | 3.18 | 0.04 | 1.98 | - |
| BULK ROCK | 63.43 | 1.03 | 15.10 | 0.10 | 10.00 | 0.11 | 3.73 | 0.41 | 0.93 | 3.18 | - | 1.98 | 100.00 |

*Major oxides calculated using mineral volume percentages after Friedman (1960). To estimate Fe₂O₃ content, we assumed realistic Fe³⁺/Fe^T values of 0.08 for biotite, 0.05 for ilmenite and 0.00 for garnet in the calculation.

§XRF data recalculated to 100% with iron distributed into ferric and ferrous oxides based on the petrographic derived ratio.

Figure 4 is a P - T pseudosection depicting mineral equilibria appropriate for the bulk rock composition in Table 2, subsequent to major prograde dehydration-melting reactions and melt loss events (cf. Thompson, 1982; White and Powell, 2002). In this model, the preserved assemblage of K-feldspar–garnet–quartz–sillimanite–biotite–ilmenite–rutile is stable in a narrow pentavariant field from 8 to 9 kbar and 760 to 790°C. This pressure constraint is based largely on the position of the reaction boundary for rutile growth, which varies according to poorly known Fe₂O₃ content (Fig. 4). A more conservative P estimate of 6–9 kbar, at say 775°C, is made by considering the absence of cordierite and kyanite in the rock.

Figures 5a–5h show mineral abundance isopleths (in mol. proportions) for each phase of concern over the relevant P - T space. At the inferred equilibrium conditions (indicated by a star), the predicted mineral abundances are approximately equal to those actually observed in the rock (Table 1). For example, predicted/observed amounts for garnet are 30/33 mol.%; K-feldspar, 28/26 mol.%; quartz, 18/19 mol.%; sillimanite, 13/16 mol.%; liquid, 7/0 mol.%; biotite, 2/3 mol.%; ilmenite, 2/2 mol.%, and; rutile 0.2/0.2 mol.%. According to the logic of Stüwe and Powell (1995), this result suggests that the preserved assemblage probably did not undergo any significant re-equilibration after crystallising at around 8–9 kbar and 760–790°C. Minor discrepancies between the observed and predicted amounts of each phase may be attributable to inaccuracies in the bulk composition, some of which could be a function of garnet fractionation from the system (cf. Stüwe, 1997). As a relevant example, Figure 6 shows a T - X_{EBC} pseudosection in which some almandine forming elements (mainly Fe) are removed from the bulk chemistry, with a predicted increase in sillimanite abundance because of the effective increase in Al.

Interpretative P - T paths for biotite, sillimanite and rutile growth are shown in Figures 5c, e and g, near to the inferred equilibration conditions. It is deduced that late

biotite growth, albeit minor, must have proceeded along a cooling path. However, the predicted increase in biotite of up to 7 mol.% during cooling from 790 to 760°C

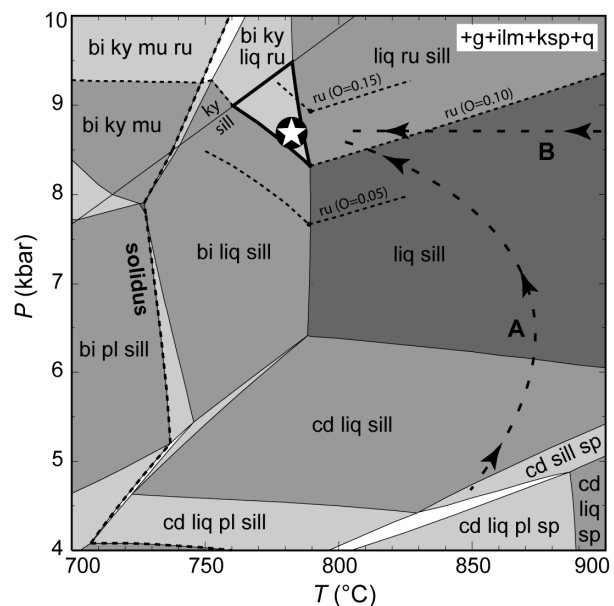


Figure 4. P - T pseudosection in MnNCKFMASHTO for the bulk composition: MnO=0.11, Na₂O=0.93, Ca=0.41, K₂O=3.18, FeO=10.01, MgO=3.72, Al₂O₃=15.10, SiO₂=63.43, H₂O=1.03, Fe₂O₃=0.10. The assemblage of interest in this study is indicated by the star. Zero molar abundance isopleths for rutile are depicted for varying Fe₂O₃ values of 0.05 mol.%, 0.10 mol.% and 0.15 mol.%. The arrowed lines (labeled A and B) represent hypothetical P - T paths on the basis of relic spinel inclusions in garnet, emanating from lower P (path A) or substantially higher T (path B). Mineral abbreviations: bi, biotite; cd, cordierite; g, garnet; ilm, ilmenite; ksp, K-feldspar; ky, kyanite; liq, liquid; mu, muscovite; pl, plagioclase; q, quartz; ru, rutile; sill, sillimanite; sp, spinel.

implies a greater amount of retrograde hydration than is observed in the rock, and that H₂O content is slightly overestimated in our model. An overestimate of H₂O also explains the predicted 7 mol.% of a liquid phase (Fig. 5a), which does not necessarily signify congealed melt *in situ* (cf. Brown, 2002). Again, the very low amount of observed biotite (~3 mol.%) and lack of any evidence for substantial rehydration suggests that most melt migrated

out of the equilibration volume considered in this study (Spear et al., 1999; White and Powell, 2002). The growth of sillimanite could reflect a former increase in *P*, in accord with the production of rutile. In addition, the microstructural evidence for continued growth of sillimanite relative to garnet (Fig. 5b) seems consistent with a component of cooling in the *P*-*T* path.

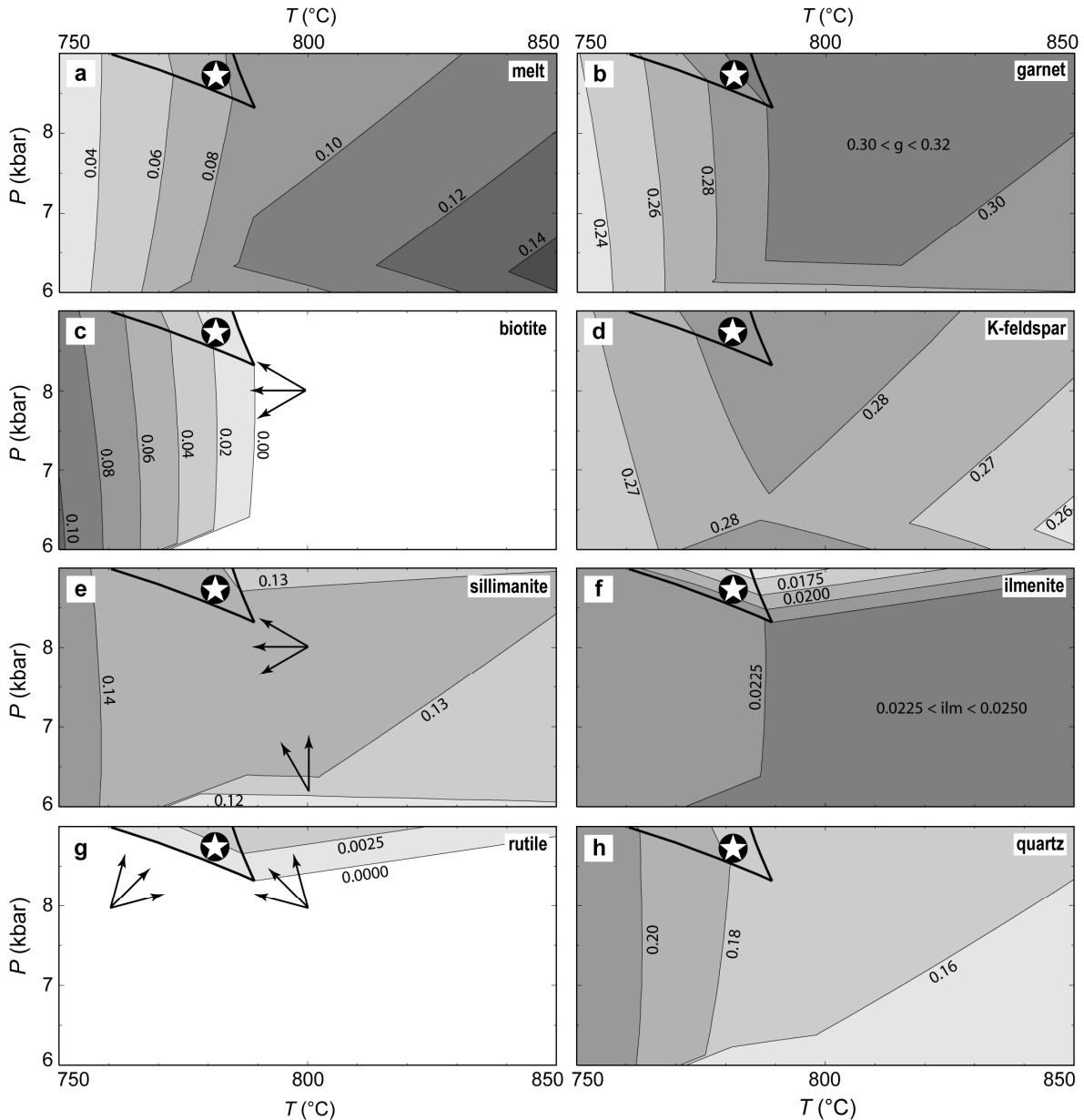


Figure 5. Molar abundance isopleths for the relevant phases (a–h) shown on a portion of the *P*-*T* pseudosection in Figure 4. The isopleth values at the star, appropriate to the observed assemblage, are: melt=0.07, garnet=0.30, biotite=0.02, K-feldspar=0.28, sillimanite=0.13, ilmenite=0.02, rutile=0.002, and, quartz=0.18 q. Arrows in (c), (e) and (g) indicate *P*-*T* paths over which biotite, sillimanite and rutile will grow in the vicinity of the observed assemblage.

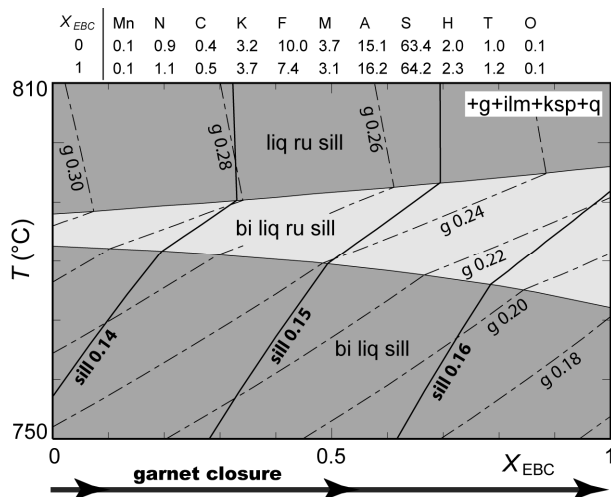


Figure 6. T - X_{EBC} pseudosection at 8.5 kbar in the system MnNCKFMASHTO. $X_{EBC} = 0$ represents the bulk composition used in this study, whereas values of X_{EBC} between 0 and 1 reflect effective bulk compositions (EBC) that account for increasing garnet closure from the chemical system. Modal isopleths are shown for sillimanite (solid lines) and garnet (dashed lines). In this example, the proportion of sillimanite increases as a function of garnet closure.

Discussion

The estimated equilibration conditions of 8–9 kbar and 760–790°C for metapelitic gneiss from Clemence Massif are consistent with parts of the adjacent Amery Ice Shelf region and Northern PCM (Fig. 1). Most notably, they are comparable to conditions of ~7–7.5 kbar and ~800°C recognised for Jetty Peninsula (Hand et al., 1994), and of ~7–10 kbar and ~800–900°C for the Reinbolt Hills (Nichols and Berry, 1991; Ziemann et al., 2005). Additionally, metapelitic gneisses from these localities contain near-peak assemblages involving garnet–sillimanite–quartz–K-feldspar–ilmenite–rutile (plus biotite and plagioclase at Reinbolt Hills), that are similar to our sample from Clemence Massif (Nichols and Berry, 1991; Hand et al., 1994).

Another reason for comparing the metamorphism of Clemence Massif with Jetty Peninsula is that, to the best of our knowledge, they are the only localities within the PCM that show any evidence of a substantial ~500 Ma thermal event overprinting Grenville-age rocks. Petrographically similar gneissose leucogranites (or leucogneisses) from each locality have yielded virtually identical U-Pb zircon ages of 940–910 Ma (Manton et al., 1992; Corvino et al., 2005) that reflect the timing of granulite-facies reworking in the adjoining Northern PCM (e.g. Kinny et al., 1997; Boger et al., 2000; Carson et al., 2000). However, the leucogranites were also affected by a thermal event at ~500 Ma, as shown by lower intercept and concordant zircon ages (Manton et al., 1992; Corvino et al., 2005), that is not apparent in the Northern PCM.

Although the effect of a ~500 Ma thermal event on metapelitic gneisses from Jetty Peninsula could be indicated by the growth of secondary cordierite–hercynite symplectites (Hand et al., 1994; Scrimgeour and Hand, 1997), such reaction microstructures are not evident in our sample. An important difference is that we observe hercynite as relic inclusions in garnet. The petrogenetic grids of, for example, Bohlen et al. (1986), Hensen (1986) and Clarke et al. (1989), suggest that this is most likely the result of an anticlockwise P - T - t path. In which case, the metamorphic evolution of Clemence Massif might be better compared to parts of the Northern PCM further to the west of Jetty Peninsula, where metapelitic granulites reworked at ~1000 Ma also record anticlockwise P - T paths (Thost and Hensen, 1992; Boger and White, 2003). Nonetheless, properly delineating an anticlockwise P - T path for our sample is problematic because (i) reaction microstructures are generally lacking, and (ii) the primary hercynite may have been stable at substantially lower T , and higher P , owing to its Zn content (Nichols et al., 1992).

Relating the observations made here to the ~1000 Ma and ~500 Ma radiogenic ages for Clemence Massif is not straightforward (Tingey, 1991; Corvino et al., 2005). Perhaps the simplest interpretation is to consider that the relic spinel inclusions reflect the ~1000 Ma event, and that the assemblage of K-feldspar–garnet–quartz–sillimanite–biotite–ilmenite–rutile equilibrated during the ~500 Ma event. However, if our particular rock was thoroughly dehydrated by melt loss during a ~1000 Ma granulite-facies event, then it may arguably record little microstructural evidence of a subsequent high-grade event at ~500 Ma (cf. White and Powell, 2002). The preserved assemblage could, therefore, be a ~1000 Ma product entirely. Another possibility is that the protolith of the metapelite has a Neoproterozoic depositional age, in which case the high-grade metamorphism would have occurred at ~500 Ma.

Acknowledgements. This work is a result of the 2002-03 Prince Charles Mountains Expedition of Germany and Australia (PCMEGA), funded by the Australian Antarctic Division (AAD) and the German Federal Republic Geological Survey (Bundesanstalt für Geowissenschaften und Rohstoffe, BGR). The participants of the 2002-03 PCMEGA and ANARE are thanked for their logistic support and friendship in Antarctica. We express our thanks to Geoff Clarke and Chris Carson for constructive reviews that helped improve this manuscript. Paul Fitzgerald is thanked for his editorial handling. A.F.C. acknowledges the financial support of a Melbourne Research Scholarship provided by The University of Melbourne.

References

- Boger, S. D., C. J. Carson, C. J. L. Wilson, and C. M. Fanning (2000), Neoproterozoic deformation in the Radok Lake region of the northern Prince Charles Mountains, east Antarctica; evidence for a single protracted orogenic event, *Precambrian Research*, 104, 1–24.
- Boger, S. D., and R. W. White (2003), The metamorphic evolution of metapelitic granulites from Radok Lake, northern Prince Charles Mountains, east Antarctica; evidence for an anticlockwise P - T path, *Journal of Metamorphic Geology*, 21, 285–298.
- Bohlen, S. R., W. A. Dollase, and V. J. Wall (1986), Calibration and applications of spinel equilibria in the system FeO - Al_2O_3 - SiO_2 , *Journal of Petrology*, 27, 1143–1156.

- Brown, M. (2002), Retrograde processes in migmatites and granulites revised, *Journal of Metamorphic Geology*, 20, 25–40.
- Carson, C. J., S. D. Boger, C. M. Fanning, C. J. L. Wilson and D. Thost (2000), SHRIMP U-Pb geochronology from Mt. Kirkby, northern Prince Charles Mountains, East Antarctica, *Antarctic Science*, 12, 429–442.
- Carver, R. E. (1971), *Procedures in Sedimentary Petrology*, John Wiley and Sons Inc., New York, 653 p.
- Cesare, B., S. Meli, and L. Nodari (2005), Fe³⁺ reduction during biotite melting in graphitic metapelites: another origin of CO₂ in granulites, *Contributions to Mineralogy and Petrology*, 149, 129–140.
- Clarke, G. L., R. Powell, and M. Guiraud (1989), Low-pressure granulite facies metapelitic assemblages and corona textures from MacRoberston Land, east Antarctica: the importance of Fe₂O₃ and TiO₂ in accounting for spinel-bearing assemblages, *Journal of Metamorphic Geology*, 7, 323–335.
- Coggon, R. and T. J. B. Holland (2002), Mixing properties of phengitic micas and revised garnet-phengite thermobarometers, *Journal of Metamorphic Geology*, 20, 683–696.
- Corvino, A. F., S. D. Boger, C. J. L. Wilson, and I.C.W. Fitzsimons (2005), Geology and SHRIMP U-Pb zircon chronology of the Clemence Massif, Central Prince Charles Mountains, East Antarctica, *Terra Antarctica*, 12, 55–68.
- Deer, W. A., R. A. Howie, and J. Zussman (1992), *An Introduction to the Rock Forming Minerals - 2nd ed*, Pearson Education Limited, Harlow, England, 696 p.
- Dyar, M.D., E.W. Lowe, C.V. Guidotti, and J. S. Delaney (2002), Fe³⁺ and Fe²⁺ partitioning among silicates in metapelites: A synchrotron micro-XANES study, *American Mineralogist*, 87, 514–522.
- Friedman, G. M. (1960), Chemical analyses of rocks with the petrographic microscope, *American Mineralogist*, 45, 69–78.
- Fyfe, W. S. (1973), *The Granulite Facies, Partial Melting and the Archaean Crust*, Philosophical Transactions for the Royal Society of London. Series, A273, 457–461.
- Guidotti, C. V., and M. D. Dyar (1991), Ferric iron in metamorphic biotite and its petrologic and crystallochemical implications, *American Mineralogist*, 76, 161–175.
- Hand, M., I. Scrimgeour, R. Powell, K. Stüwe, and C. J. L. Wilson (1994), Metapelitic granulites from Jetty Peninsula, east Antarctica: formation during a single event or by polymetamorphism?, *Journal of Metamorphic Geology*, 12, 557–573.
- Hensen, B. J. (1986), Theoretical phase relations involving cordierite and garnet revisited: the influence of oxygen fugacity on the stability of sapphirine and spinel in the system Mg–Fe–Al–Si–O, *Contributions to Mineralogy and Petrology*, 92, 362–367.
- Holland, T. J. B., and R. Powell (1998), An internally consistent thermodynamic data set for phases of petrological interest, *Journal of Metamorphic Geology*, 16, 309–343.
- Johnson, S. E., and R. H. Vernon (1995), Inferring the timing of porphyroblast growth in the absence of continuity between inclusion trails and matrix foliations: can it be reliably done?, *Journal of Structural Geology*, 17, 1203–1206.
- Kinny, P. D., L. P. Black, and J. W. Sheraton (1997), Zircon U-Pb ages and geochemistry of igneous and metamorphic rocks in the northern Prince Charles Mountains, AGSO *Journal of Australian Geology & Geophysics*, 16, 637–654.
- Krynauw, J. R. (1996), A review of the geology of East Antarctica, with special reference to the c. 1000 Ma and c. 500 Ma events, *Terra Antarctica*, 3, 77–89.
- Manton, W. I., E. S. Grew, J. Hofmann, and J. W. Sheraton (1992), Granitic rocks of the Jetty Peninsula, Amery Ice Shelf area, East Antarctica, in *Recent Progress in Antarctic Earth Science*, edited by Yoshida, Y., K. Kaminuma, and K. Shiraishi, Terra Scientific Publishing Company, Tokyo, 179–189.
- Mahar, E. M., J. M. Baker, R. Powell, T. J. B. Holland, and N. Howell (1997), The effect of Mn on mineral stability in metapelites, *Journal of Metamorphic Geology*, 15, 223–238.
- McLeod, I. R., (1959), Report on geological and glaciological work by the 1958 Australian National Antarctic Research Expedition, Bureau of Mineral Resources Australia, Record 1959/131.
- Mikhalsky, E. V., J. W. Sheraton, A. A. Laiba, R. J. Tingey, D. E. Thost, E. N. Kamenev, and L. V. Fedorov (2001), Geology of the Prince Charles Mountains, Antarctica, AGSO – Geoscience Australia, Canberra, bulletin 247.
- Nichols, G. T., and R. F. Berry (1991), A decompressional *P–T* path, Reinbolt Hills, East Antarctica, *Journal of Metamorphic Geology*, 9, 257–266.
- Nichols, G. T., R. F. Berry, and D. H. Green (1992), Internally consistent gahnitic spinel-cordierite-garnet equilibria in the FMASHZn system: geothermobarometry and applications, *Contributions to Mineralogy and Petrology*, 111, 362–377.
- Powell, R. (1983), Processes in Granulite-facies Metamorphism, in *Migmatites, Melting and Metamorphism*, edited by Atherton, M. P., and C. D. Gribble, Shiva, Nantwich, United Kingdom, 127–139.
- Powell, R., and T. J. B. Holland (1988), An internally consistent thermodynamic dataset with uncertainties and correlations: 3. Application methods, worked examples and a computer program, *Journal of Metamorphic Geology*, 6, 173–204.
- Powell, R., T. Holland, and B. Worley (1998), Calculating phase diagrams involving solid solutions via non-linear equations, with examples using THERMOCALC, *Journal of Metamorphic Geology*, 16, 577–588.
- Scrimgeour, I., and M. Hand (1997), A metamorphic perspective on the Pan-African overprint in the Amery area of Mac. Robertson Land, East Antarctica, *Antarctic Science*, 9, 313–335.
- Shau, Y., H. Yang, and D. R. Peacor (1991), On oriented titanite and rutile inclusions in sagentic biotite, *American Mineralogist*, 76, 1205–1217.
- Sheraton, J. (1980), Geochemistry of Precambrian metapelites from East Antarctica: secular and metamorphic variations, *BMR Journal of Australian Geology and Geophysics*, 5, 279–288.
- Spear, F. S., M. J. Kohn, and J. T. Cheney (1999), *P–T* paths from anatectic pelites, *Contributions to Mineralogy and Petrology*, 134, 17–32.
- Stüwe, K., and R. Powell (1995), *PT* paths from modal proportions: applications to the Koralm Complex, Eastern Alps, *Contributions to Mineralogy and Petrology*, 119, 83–93.
- Stüwe, K. (1997), Effective bulk composition changes due to cooling: a model predicting complexities in retrograde reaction textures, *Contributions to Mineralogy and Petrology*, 129, 43–52.
- Thompson, A. B. (1982), Dehydration melting of pelitic rocks and the generation of H₂O-undersaturated granitic liquids, *American Journal of Science*, 282, 1567–1595.
- Thost, D. E., and B. J. Hensen (1992), Gneisses of the Porthos and Athos Ranges, Northern Prince Charles Mountains, East Antarctica: Constraints on the prograde and retrograde *P–T* path, in *Recent Progress in Antarctic Earth Science*, edited by Yoshida, Y., K. Kaminuma, and K. Shiraishi, Terra Scientific Publishing Company, Tokyo, 93–102.
- Tingey, R. J., R. N. England, and J. W. Sheraton (1981), Geological investigations in Antarctica 1973 – the southern Prince Charles Mountains, Bureau of Mineral Resources Australia, Record 1981/43.
- White, R. W., and R. Powell (2002), Melt loss and the preservation of granulite facies mineral assemblages, *Journal of Metamorphic Geology*, 20, 621–632.
- White, R. W., R. Powell, and T. J. B. Holland (2001), Calculation of partial melting equilibria in the system Na₂O–CaO–K₂O–FeO–MgO–Al₂O₃–SiO₂–H₂O (NCKFMASH), *Journal of Metamorphic Geology*, 19, 139–153.
- White, R. W., R. Powell, and G. L. Clarke (2002), The interpretation of reaction textures in Fe-rich metapelitic granulites of the Musgrave Block, central Australia: constraints from mineral equilibria calculations in the system K₂O–FeO–MgO–Al₂O₃–SiO₂–H₂O–TiO₂–Fe₂O₃, *Journal of Metamorphic Geology*, 20, 41–55.
- White, R. W., N. E. Pomroy, and R. Powell (2005), An *in situ* metatexite-diatexite transition in upper amphibolite facies rocks from Broken Hill, Australia, *Journal of Metamorphic Geology*, 23, 579–602.
- Yoshida, M., J. Jacobs, M. Santosh, and H. M. Rajesh (2003), Role of Pan-African events in the Circum-East Antarctic Orogen of East Gondwana: a critical overview, in *Proterozoic East Gondwana*:

Supercontinent Assembly and Breakup, edited by Yoshida M., B. F. Windley, and S. Dasgupta, Geological Society, London, Special Publications, 206, 57–75.

Ziemann, M. A., H-J. Förster, D. E. Harlov, and D. Frei (2005), Origin of fluorapatite-monzite assemblages in a metamorphosed,

sillimanite-bearing pegmatoid, Reinbolt Hills, East Antarctica, European Journal of Mineralogy, 17, 567–579.

Zeh, A. and M. B. Holness (2003), The effect of reaction overstep on garnet microtextures in metapelitic rocks of the Ilesha Schist Belt, SW Nigeria, Journal of Petrology, 44, 967–994.

Appendix A. Mineral properties table

Table A1. Listing of some mineral properties used in this study. All data is from Holland and Powell (1998), except specific gravity values which are taken from Deer et al. (1992). The effective volumes for garnet and biotite are the averaged molar volumes for the different end-members of those minerals (following Stüwe and Powell, 1995).

| Mineral | Formula | Symbol | Specific gravity | Volume J bar ⁻¹ | Effective volume | No. of oxides |
|-------------|--|--------|------------------|----------------------------|------------------|---------------|
| K-feldspar | KAlSi ₃ O ₈ | ksp | 2.6 | 10.900 | 10.900 | 4 |
| Quartz | SiO ₂ | q | 2.7 | 2.269 | 2.269 | 1 |
| Garnet | | g | 4.0 | | 11.435 | 7 |
| Almandine | Fe ₃ Al ₂ Si ₃ O ₁₂ | alm | | 11.551 | | |
| Pyrope | Mg ₃ Al ₂ Si ₃ O ₁₂ | py | | 11.318 | | |
| Sillimanite | Al ₂ SiO ₅ | sill | | 4.986 | 4.986 | 2 |
| Biotite | | bi | 3.0 | | 15.198 | 7 |
| Annite | KFe ₃ AlSi ₃ O ₁₀ (OH) ₂ | ann | | 15.432 | | |
| Phlogopite | KMg ₃ AlSi ₃ O ₁₀ (OH) ₂ | phl | | 14.964 | | |
| Ilmenite | FeTiO ₃ | ilm | 4.7 | 3.169 | 3.169 | 2 |
| Rutile | TiO ₂ | ru | 4.8 | 1.882 | 1.882 | 1 |

Appendix B. Mineral chemistry tables

Table B1. Chemical analyses of garnet (g) and biotite (bi). $X_{Mg} = Mg/(Fe^T + Mg)$. Coexisting mineral pairs are included in square brackets.

| | g1 core | g1 rim | g2 core | g3[ilm2] | g4[bi2] | g5 | g6 | bi1 | bi2[g4] | bi3 | bi4 | bi5 |
|--------------------------------|-----------|--------|---------|----------|---------|--------|-----------|-------|---------|-------|-------|-------|
| SiO ₂ | 38.44 | 38.39 | 37.59 | 36.45 | 37.40 | 37.43 | 37.55 | 35.72 | 35.67 | 35.08 | 37.59 | 37.44 |
| TiO ₂ | 0.02 | 0.03 | 0.04 | 0.05 | 0.04 | 0.03 | 0.01 | 6.34 | 5.55 | 4.58 | 3.60 | 3.38 |
| Al ₂ O ₃ | 21.55 | 21.61 | 21.66 | 21.47 | 21.46 | 21.71 | 21.69 | 16.80 | 16.25 | 15.81 | 17.34 | 16.84 |
| Cr ₂ O ₃ | 0.00 | 0.05 | 0.05 | 0.02 | 0.09 | 0.06 | 0.02 | 0.14 | 0.13 | 0.20 | 0.13 | 0.15 |
| FeO ^T | 32.56 | 32.30 | 33.01 | 32.75 | 33.22 | 33.07 | 33.14 | 18.03 | 17.56 | 16.26 | 13.22 | 11.66 |
| MnO | 0.51 | 0.54 | 0.54 | 0.54 | 0.56 | 0.56 | 0.56 | 0.01 | 0.01 | 0.02 | 0.00 | 0.00 |
| MgO | 6.59 | 6.52 | 6.30 | 6.46 | 6.06 | 6.38 | 6.31 | 10.86 | 10.69 | 12.87 | 15.33 | 17.45 |
| CaO | 1.06 | 1.04 | 1.14 | 1.13 | 1.13 | 1.15 | 1.15 | 0.00 | 0.00 | 0.00 | 0.00 | 0.02 |
| Na ₂ O | 0.07 | 0.06 | 0.01 | 0.02 | 0.03 | 0.05 | 0.04 | 0.18 | 0.14 | 0.11 | 0.12 | 0.15 |
| K ₂ O | 0.01 | 0.00 | 0.02 | 0.01 | 0.03 | 0.00 | 0.02 | 9.24 | 9.31 | 8.93 | 9.01 | 9.65 |
| ZnO | 0.07 | 0.00 | 0.06 | 0.02 | 0.03 | 0.07 | 0.00 | 0.01 | 0.13 | 0.00 | 0.00 | 0.08 |
| Total | 100.87 | 100.53 | 100.42 | 98.92 | 100.04 | 100.49 | 100.48 | 97.36 | 95.44 | 93.86 | 96.36 | 96.82 |
| | 24 O apfu | | | | | | 22 O apfu | | | | | |
| Si | 6.00 | 6.00 | 5.92 | 5.84 | 5.93 | 5.90 | 5.92 | 5.30 | 5.40 | 5.37 | 5.47 | 5.42 |
| Ti | 0.00 | 0.00 | 0.00 | 0.01 | 0.00 | 0.00 | 0.00 | 0.71 | 0.63 | 0.53 | 0.39 | 0.37 |
| Al | 3.97 | 3.98 | 4.02 | 4.06 | 4.01 | 4.03 | 4.03 | 2.94 | 2.90 | 2.85 | 2.97 | 2.87 |
| Cr | 0.00 | 0.01 | 0.01 | 0.00 | 0.01 | 0.01 | 0.00 | 0.02 | 0.02 | 0.02 | 0.01 | 0.02 |
| Fe ^T | 4.25 | 4.23 | 4.35 | 4.39 | 4.40 | 4.36 | 4.37 | 2.24 | 2.22 | 2.08 | 1.61 | 1.41 |
| Mn | 0.07 | 0.07 | 0.07 | 0.07 | 0.07 | 0.07 | 0.08 | 0.00 | 0.00 | 0.00 | 0.00 | 0.00 |
| Mg | 1.53 | 1.52 | 1.48 | 1.54 | 1.43 | 1.50 | 1.48 | 2.40 | 2.41 | 2.93 | 3.33 | 3.76 |
| Ca | 0.18 | 0.17 | 0.19 | 0.19 | 0.19 | 0.19 | 0.19 | 0.00 | 0.00 | 0.00 | 0.00 | 0.00 |
| Na | 0.02 | 0.02 | 0.00 | 0.01 | 0.01 | 0.01 | 0.01 | 0.05 | 0.04 | 0.03 | 0.03 | 0.04 |
| K | 0.00 | 0.00 | 0.00 | 0.00 | 0.01 | 0.00 | 0.00 | 1.75 | 1.80 | 1.74 | 1.67 | 1.78 |
| Zn | 0.01 | 0.00 | 0.01 | 0.00 | 0.00 | 0.01 | 0.00 | 0.00 | 0.01 | 0.00 | 0.00 | 0.01 |
| Total | 16.03 | 16.01 | 16.06 | 16.12 | 16.07 | 16.09 | 16.08 | 15.41 | 15.43 | 15.56 | 15.49 | 15.68 |
| X_{Mg} | 0.27 | 0.26 | 0.25 | 0.26 | 0.25 | 0.26 | 0.25 | 0.52 | 0.52 | 0.59 | 0.67 | 0.73 |

Table B2. Chemical analyses of K-feldspar (ksp), ilmenite (ilm), rutile (ru) and spinel (sp). Coexisting mineral pairs are included in square brackets.

| | ksp1 | ksp2 | ksp3 | ilm1 | ilm2[g3] | ru1 | ru2 | sp1 | sp2 |
|--------------------------------|-----------|-------|--------|---------|----------|----------|-------|-----------|-------|
| SiO ₂ | 64.68 | 65.02 | 67.19 | 0.00 | 0.00 | 0.00 | 0.00 | 0.00 | 0.00 |
| TiO ₂ | 0.02 | 0.03 | 0.04 | 53.21 | 52.98 | 97.03 | 94.73 | 0.02 | 0.00 |
| Al ₂ O ₃ | 19.20 | 19.31 | 19.29 | 0.00 | 0.02 | 0.10 | 0.09 | 57.87 | 58.29 |
| Cr ₂ O ₃ | 0.00 | 0.02 | 0.00 | 0.04 | 0.02 | 0.04 | 0.14 | 0.67 | 0.55 |
| FeO ^T | 0.00 | 0.00 | 0.00 | 47.07 | 45.40 | 0.47 | 0.90 | 21.58 | 23.24 |
| MnO | 0.00 | 0.00 | 0.03 | 0.23 | 0.19 | 0.03 | 0.02 | 0.02 | 0.01 |
| MgO | 0.02 | 0.00 | 0.00 | 0.05 | 0.32 | 0.01 | 0.01 | 6.41 | 6.44 |
| CaO | 0.12 | 0.10 | 0.11 | 0.00 | 0.00 | 0.02 | 0.01 | 0.00 | 0.01 |
| Na ₂ O | 1.99 | 1.98 | 1.79 | 0.00 | 0.01 | 0.03 | 0.03 | 0.41 | 0.36 |
| K ₂ O | 13.44 | 13.42 | 14.10 | 0.00 | 0.01 | 0.01 | 0.01 | 0.01 | 0.01 |
| ZnO | 0.00 | 0.02 | 0.00 | 0.05 | 0.00 | 0.00 | 0.00 | 10.20 | 9.04 |
| Total | 99.89 | 99.89 | 102.56 | 100.67 | 98.95 | 97.73 | 95.93 | 97.20 | 97.97 |
| | 32 O apfu | | | 6 Oapfu | | 2 O apfu | | 32 O apfu | |
| Si | 11.90 | 11.90 | 11.98 | 0.00 | 0.00 | 0.00 | 0.00 | 0.00 | 0.00 |
| Ti | 0.00 | 0.00 | 0.00 | 2.00 | 2.02 | 1.00 | 0.99 | 0.00 | 0.00 |
| Al | 4.16 | 4.16 | 4.05 | 0.00 | 0.00 | 0.00 | 0.00 | 15.74 | 15.72 |
| Cr | 0.00 | 0.00 | 0.00 | 0.00 | 0.00 | 0.00 | 0.00 | 0.12 | 0.10 |
| Fe ^T | 0.00 | 0.00 | 0.00 | 1.97 | 1.92 | 0.01 | 0.01 | 4.16 | 4.45 |
| Mn | 0.00 | 0.00 | 0.00 | 0.01 | 0.01 | 0.00 | 0.00 | 0.00 | 0.00 |
| Mg | 0.01 | 0.00 | 0.00 | 0.00 | 0.02 | 0.00 | 0.00 | 2.20 | 2.20 |
| Ca | 0.02 | 0.02 | 0.02 | 0.00 | 0.00 | 0.00 | 0.00 | 0.00 | 0.00 |
| Na | 0.71 | 0.70 | 0.62 | 0.00 | 0.00 | 0.00 | 0.00 | 0.18 | 0.16 |
| K | 3.15 | 3.13 | 3.21 | 0.00 | 0.00 | 0.00 | 0.00 | 0.00 | 0.00 |
| Zn | 0.00 | 0.00 | 0.00 | 0.00 | 0.00 | 0.00 | 0.00 | 1.74 | 1.53 |
| Total | 19.95 | 19.93 | 19.90 | 3.99 | 3.98 | 1.00 | 1.00 | 24.15 | 24.16 |

Note: Compositions were obtained using a CAMECA SX-50 Electron Probe Microanalyser (operating conditions 15 kV and 25 nA probe current) at the School of Earth Sciences, The University of Melbourne, Australia.